

Article

FTIR-Based Crystallinity Assessment of Aragonite–Calcite Mixtures in Archaeological Lime Binders Altered by Diagenesis

Michael B. Toffolo ^{1,*} , Lior Regev ² , Stéphan Dubernet ¹, Yannick Lefrais ¹ and Elisabetta Boaretto ² 

¹ Institut de Recherche sur les Archéomatériaux-Centre de Recherche en Physique Appliquée à l'Archéologie (IRAMAT-CRP2A), UMR 5060 CNRS, Université Bordeaux Montaigne, 8 Esplanade des Antilles, 33607 Pessac, France; stephan.dubernet@u-bordeaux-montaigne.fr (S.D.); yannick.lefrais@u-bordeaux-montaigne.fr (Y.L.)

² D-REAMS Radiocarbon Dating Laboratory, Weizmann Institute of Science, 234 Herzl Street, Rehovot 7610001, Israel; lior.regev@weizmann.ac.il (L.R.); elisabetta.boaretto@weizmann.ac.il (E.B.)

* Correspondence: michael.toffolo@u-bordeaux-montaigne.fr; Tel.: +33-557-124-681

Received: 10 January 2019; Accepted: 15 February 2019; Published: 18 February 2019



Abstract: Lime plaster and mortar are pyrotechnological materials that have been employed in constructions since prehistoric times. They may nucleate as calcite and/or aragonite under different environmental settings. In nature, aragonite and calcite form through biogenic and geogenic processes that lead to different degrees of atomic order. The latter is a result of defects in the crystal lattice, which affect the properties of crystals, including their interaction with infrared light. Using Fourier transform infrared spectrometry (FTIR) with the KBr pellet method, it is possible to exploit these differences and assess the degree of atomic order of aragonite and calcite crystals and thus their mechanisms of formation. Here we use FTIR to characterize the degree of short-range atomic order of a pyrogenic form of aragonite recently observed in experimental and archaeological lime binders. We show that pyrogenic aragonite has a unique signature that allows its identification in archaeological sediments and lime binders of unknown origin. Based on these results, we developed a new FTIR-based method to assess the integrity and degree of preservation of aragonite and calcite when they occur together in the same material. This method allowed a better assessment of the diagenetic history of an archaeological plaster and finds application in the characterization of present-day conservation materials, such as lime plaster and mortar, where different polymorphs may nucleate and undergo recrystallization processes that can alter the mechanical properties of binders.

Keywords: lime; plaster; mortar; carbonate; calcite; aragonite; radiocarbon; FTIR; XRD; diagenesis

1. Introduction

Anthropogenic carbonates are human-made materials composed of CaCO_3 that derive from pyrotechnological processes and include ash, lime plaster, lime mortar and, to a lesser extent, concrete [1–4]. These are among the most common materials produced by humans since prehistoric times [2]. Lime plaster and mortar are still largely used today in conservation works, with decorative (e.g., coating) or structural (e.g., binder between cobbles) functions [5–7]. Their physical and chemical properties are determined by the raw materials and lime technology used in their production, as well as by their functional role and environmental conditions upon and after setting [8–10]. Therefore, their characterization is crucial in the interpretation of the archaeological record, in the study of historic buildings, and in the development of novel construction materials and restoration strategies.

Lime binders usually nucleate as calcite, the stable polymorph of CaCO_3 at ambient temperatures and pressures, upon carbonation of CaO (quicklime) and Ca(OH)_2 (hydrated lime) [1,11]. It has been recently shown that the same mechanism of formation can lead to the nucleation of aragonite, one of the metastable polymorphs of CaCO_3 , in different amounts based on the starting CaCO_3 substrate and environmental settings in magnesium-free lime plasters [12]. In nature, aragonite and calcite may form through different processes, such as precipitation in supersaturated solutions, precipitation in boiling water at hot springs, slow crystal growth in speleothems and spar, and biomineralization [11,13]. All of these formation processes may be conducive to different crystal shapes, from the crossed-lamellar arrangement in aragonitic shells to needle-shaped crystals in evaporites. In addition, different crystallization modes are responsible for the presence of impurities and defects in the crystal lattice of aragonite and calcite, which affect the degree of long-range atomic order of crystals and therefore their chemical and physical properties [14–18]. Among the chemical and physical properties affected by shifts in local structural order, significant changes occur in the way aragonite and calcite crystals behave when exposed to infrared light. Using Fourier transform infrared spectrometry (FTIR) with the KBr pellet method, Regev et al. [19] found that upon repeated grinding of the same pellet, the ratios of specific vibrational modes of calcite decrease, and if plotted they describe trend lines that are specific to calcites formed through different mechanisms (Figure 1). These include calcite derived from pyrotechnological processes, i.e., ash and lime plaster. Suzuki et al. [20] obtained similar results for geogenic and biogenic aragonite. More specifically, the intensities of the ν_2 and ν_4 vibrational modes are normalized to the intensity of the ν_3 mode, and the values thus obtained (called ν_2 and ν_4 normalized heights) are plotted to define a so-called infrared grinding curve. The theoretical study by Poduska et al. [21] showed that the displacement between different curves is a product of different degrees of short-range atomic order in crystals formed by different mechanisms.

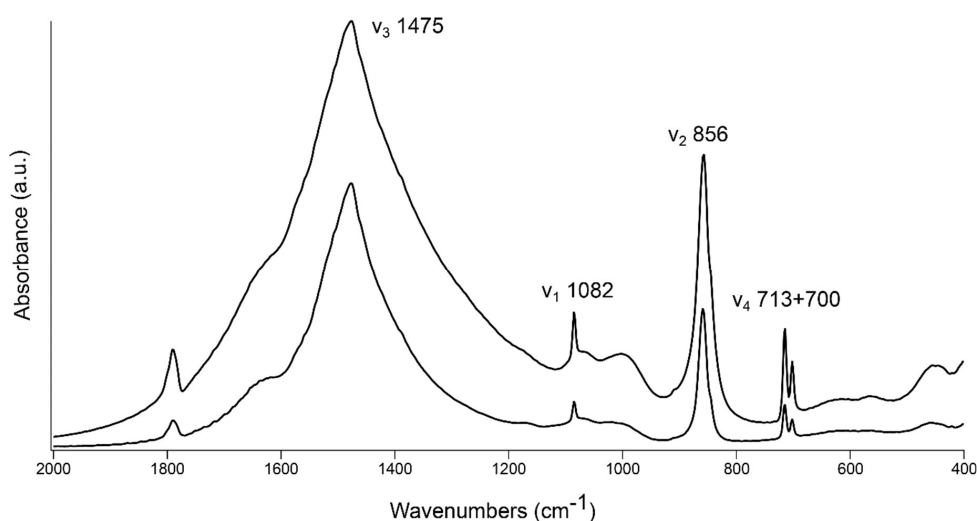


Figure 1. FTIR spectra of aragonite formed in boiling water. Upon increased grinding (lower spectrum), absorptions become narrower (a.u.: arbitrary units; spectra normalized to the ν_3 absorption of aragonite).

Infrared grinding curves of calcite and aragonite found extensive application in materials science and biomineralization [22–27]. Other fields that largely benefited from this analytical method are cultural heritage preservation and archaeology, and especially the study of anthropogenic carbonates. With grinding curves, it is possible to determine the formation process of unknown calcite crystals in sediments, artifacts and architectures, and to assess their state of preservation based on the degree of atomic order [28–33].

Since anthropogenic carbonates usually nucleate as calcite, their degree of atomic order is determined using calcite grinding curves. However, pyrogenic aragonite recently produced in experimental magnesium-free lime plasters together with calcite, and observed in archaeological

carbonate-based materials [12,31,32,34–36], has not been considered in previous infrared grinding curves. This lack of structural characterization hinders a proper assessment of the degree of preservation of lime binders comprised of aragonite–calcite mixtures, as to date there is no method for separating the contributions of the two polymorphs when they occur together in the same infrared spectrum. Therefore, the aim of this study is twofold. First, we characterize pyrogenic aragonite from the point of view of short-range atomic order using FTIR, in order to provide a means to determine the nature of aragonite crystals in archaeological materials of unknown formation or diagenetic history. Second, we propose a new method to determine the degree of atomic order, and therefore the mechanism of formation and state of preservation, of calcite and aragonite when they occur together in the same lime binder. Our results show that pyrogenic aragonite is different from all the other known forms of the mineral and exhibits a unique FTIR signature. In addition, the method proposed herein allows a rapid structural assessment of the extent of diagenesis in archaeological and present-day construction materials characterized by both aragonite and calcite, including lime plasters and mortars for radiocarbon dating.

2. Materials and Methods

2.1. Standard Reference Materials

Crystals of geogenic aragonite with well-defined crystal faces from Tazouta (Morocco) and Molina de Aragón (Spain) were purchased from Mineralogical Research Company (San Jose, CA, USA). Crystals of calcite spar from Chihuahua (Mexico) were purchased from Ward's Science (Rochester, NY, USA). Biogenic aragonite was obtained from *Glycymeris* sp. shells collected on the shore of the Mediterranean Sea at Ashkelon, Israel [37]. Aragonite precipitated out of boiling water was recovered from a kettle used over many years, where the scale was rarely removed [3]. Evaporitic aragonite was collected from the Lake Lisan Formation of the Dead Sea, Israel [38]. Pyrogenic aragonite was produced by heating powdered *Glycymeris* sp. shells to 900 °C for 12 h to obtain quicklime (CaO), which was then left to react with the atmosphere at room temperature until it carbonated completely [12]. Environmental conditions such as relative humidity and CO₂ partial pressure were not monitored. The pyrogenic aragonite sample was six years old at the time of this study. Finally, archaeological samples of pyrogenic aragonite were collected from an Iron Age destruction layer at Megiddo [35], a Bronze Age combustion feature at Tell es-Safi/Gath [39,40], and Neolithic lime plaster floors at Motza [41], all of which are located in Israel.

2.2. Density Separation

Archaeological samples of ash containing calcite and aragonite were treated following the procedure of Toffolo et al. [35] to isolate aragonite crystals from the rest of the matrix and thus analyze them using FTIR without contributions from calcite. The high specific gravity of aragonite (2.94 g/mL) was exploited to separate it from calcite (2.71 g/mL). Samples were placed in a solution of sodium polytungstate (3Na₂WO₄·9WO₃·H₂O; TC-Tungsten Compounds GmbH, Grub am Forst, Germany) and 1 mol/L sodium phosphate dibasic (Na₂HPO₄; Sigma-Aldrich, St. Louis, MO, USA) at 2.75 g/mL density and pH 8 inside a plastic tube, and centrifuged. Heavier aragonite crystals migrated to the bottom of the tube. It should be noted that pyrogenic calcite and aragonite are less ordered than their geogenic counterparts, and therefore cover a wide range of specific gravities (from ~2.0 to 2.94 g/mL). However, calcite is not heavier than 2.71 g/mL, and thus it is possible to recover almost pure aragonite crystals (~1% calcite based on radiocarbon measurements and micro-XRD; [35]) between 2.75 and 2.94 g/mL.

2.3. Scanning Electron Microscopy (SEM)

Powdered aliquots of kettle, Lisan and pyrogenic (experimental and archaeological) aragonite were placed on carbon tape and coated using a gold sputter coater Emscope SC500. Samples were

analyzed using a JEOL JSM-6460LV scanning electron microscope (JEOL, Tokyo, Japan) at 20 kV using a secondary electron detector. Megiddo ash samples were placed on carbon tape and coated using a gold-palladium sputter coater Edwards S150, and examined with a high-resolution Zeiss Leo Supra 55VP field emission scanning electron microscope (Oberkochen, Germany) between 2 and 5 kV using a secondary electron detector.

2.4. X-ray Diffraction (XRD)

Powdered samples of archaeological ash and lime plaster were analyzed with a 300 mm radius Bruker D8 Advance goniometer (Bruker, Billerica, MA, USA) configured in Bragg-Brentano mode, under the incident X-ray doublet $\text{CuK}\alpha$ combined with a 2.6° (180 px) linear Bruker LynxEye detector. The minor phase detection with good statistics is reached by acquisition for 550 s each 0.01 points in the range $15\text{--}60^\circ$ 2θ . Oriented sample holders in PolyMethyl MethAcrylate or Si of respective diameters 25 and 20 mm were used depending on the amount of material (0.5 and 0.16 cm^3). The contributions of the continuous background and of the $\text{CuK}\alpha_2$ were removed using the Bruker DIFFRAC.EVA v.4.2 software. Mineral identification and the semi-quantitative analysis were achieved using ICDD PDF2-2004 data base patterns.

2.5. Fourier Transform Infrared Spectrometry (FTIR)

A few milligrams of each standard material were homogenized and powdered in an agate mortar and pestle. About 0.1 mg were left in the mortar and mixed with approximately 0.5 mg of KBr (FTIR grade, Sigma-Aldrich, St. Louis, MO, USA) and pressed into a 7-mm pellet using a hand press (PIKE Technologies, Fitchburg, WI, USA). For grinding curves, each pellet was measured at least five times by repetitive grinding applying increasing strength, and at least five pellets per standard were analyzed. In addition, mixed pellets were prepared by weighing powdered calcite and aragonite spar in ratios of 30:70, 50:50, and 70:30, respectively, to test the grinding curve method with mixed polymorphs. Infrared spectra were obtained at 4 cm^{-1} resolution in 32 scans within the $4000\text{--}400\text{ cm}^{-1}$ spectral range using a Bruker Alpha spectrometer. Phase identification was performed using OMNIC (version 9), standard literature [42] and the reference collection of FTIR spectra of standard materials provided by the Kimmel Center for Archaeological Science, Weizmann Institute of Science (<http://www.weizmann.ac.il/kimmel-arch/infrared-spectra-library>). The infrared grinding curve method of Suzuki et al. [20], based on previous methods by Regev et al. [19] and Poduska et al. [21], was used to determine the heights of the ν_2 and ν_4 absorptions of aragonite normalized to the height of the ν_3 absorption of aragonite. Macro Basic v. 8 was used to create a macro for the calculation of the normalized heights and thus swiftly process a large number of spectra. The ν_2/ν_3 and ν_4/ν_3 ratios were multiplied by 1000 for convenience in creating grinding curve plots. In the case of samples including both calcite and aragonite, we calculated heights using the “Peak height tool” in OMNIC.

3. Results and Discussion

3.1. FTIR Grinding Curves

Figure 2 displays the reference materials analyzed in this study to obtain and test grinding curves. Geogenic crystals grow slowly over a long time. As a result, the Tazouta and Molina de Aragón samples are large and their lattice exhibits long-range atomic order over macroscopic distances (Figure 2A,B). *Glycymeris* crystals are smaller and their nucleation is biologically regulated, thus leading to the mineralization of layers with different crystal structure and organization [13]. Note that in this study we did not differentiate between nacre, crossed lamellar, myostracum, and other portions of the shell, since usually all layers are represented in archaeological sediments and plasters, even when shells are found in small fragments (Figure 2C). Aragonite crystals formed in boiling water nucleate as small ($<1\ \mu\text{m}$), elongated rods with hexagonal cross-section and show a considerable range of sizes (Figure 2D). Lisan aragonite, which is essentially evaporitic, formed in lacustrine water rich

in magnesium, which is known to inhibit the nucleation of calcite [11]. Crystals are small, elongated rods or needles that occur in rosette-like clusters or druses (Figure 2E). Being a sedimentary material, it contains minor calcite and quartz inclusions. Pyrogenic aragonite nucleates upon carbonation of magnesium-free CaO and Ca(OH)₂ at ambient temperatures and pressures and forms small (<1 μm), elongated needles, which may occur as single crystals or in clusters and include a minor amount of calcite (Figure 2F–H) [12,35].

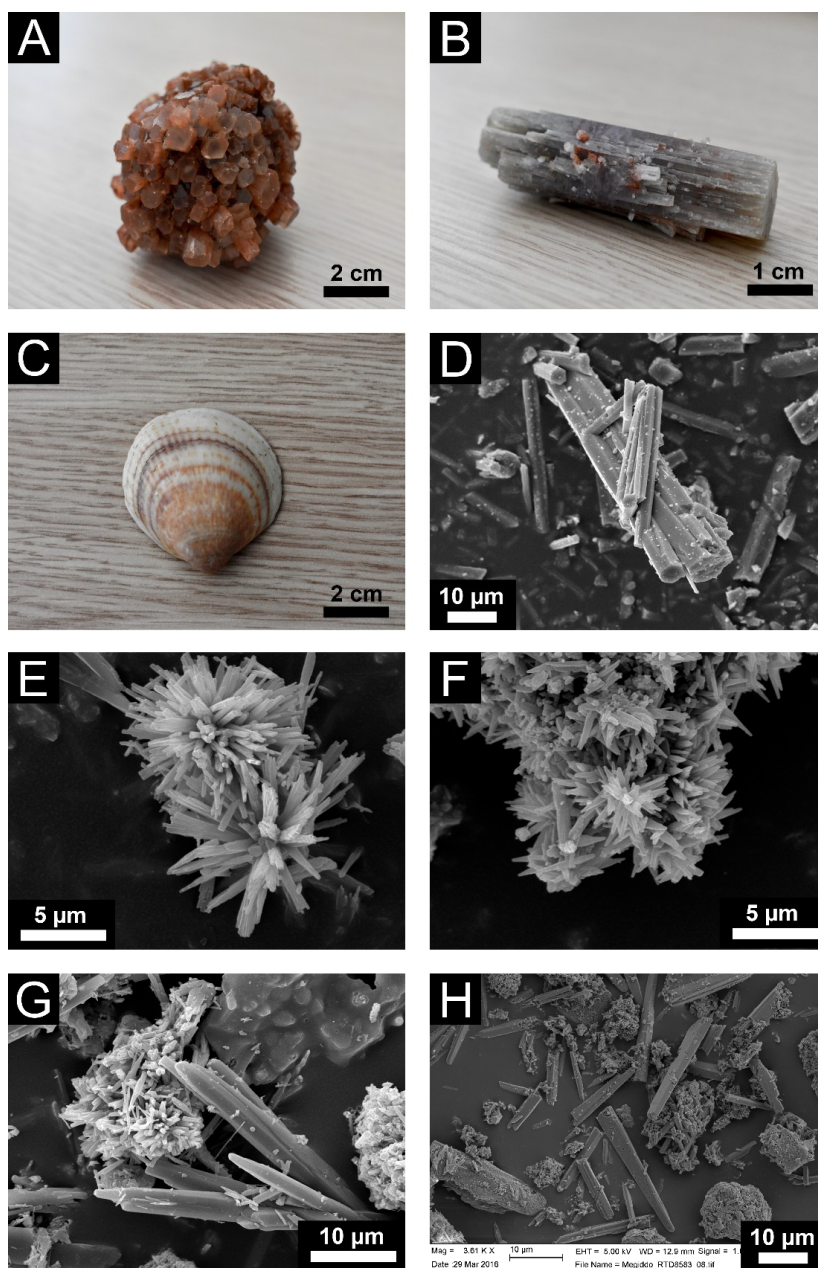


Figure 2. Materials analyzed in this study. (A) aragonite spar from Tazouta, Morocco. (B) Aragonite spar from Molina de Aragón, Spain. (C) *Glycymeris* sp. shell from Ashkelon, Israel. (D) SEM image of aragonite rods precipitated out of boiling water in a kettle. (E) SEM image of a cluster of aragonite needles precipitated out of lacustrine water in the Lake Lisan Formation at the Dead Sea, Israel. (F) SEM image of aragonite needles formed upon the carbonation of CaO and Ca(OH)₂ in an experimental quicklime. (G) SEM image of pyrogenic aragonite needles formed in high-temperature archaeological ash at Tell es-Safi/Gath, Israel. (H) SEM image of pyrogenic aragonite needles formed in high-temperature archaeological ash at Megiddo, Israel.

Figure 3 shows the plots of the ν_4 versus ν_2 normalized heights of the same sample ground repetitively using increasing strength, for all the standard materials. The two large crystals of geogenic aragonite describe similar trendlines, which exhibit the smallest slope. The trendline of biogenic aragonite from *Glycymeris* sp. shells overlaps with that of geogenic samples and continues towards lower normalized ν_2 and ν_4 values. However, the initial portion of the trendline starts below the curve of geogenic materials. Kettle aragonite is characterized by a grinding curve displaced above the previous three. The pyrogenic and Lisan curves are even more displaced and show a greater slope.

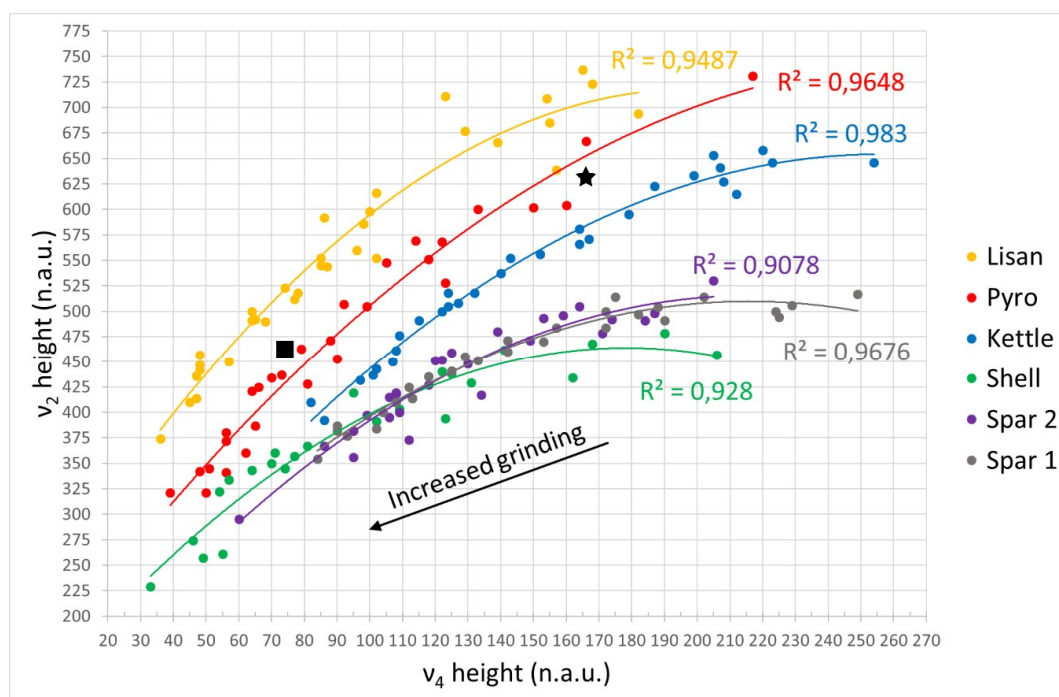


Figure 3. Aragonite grinding curves plot (n.a.u.: normalized absorbance units). Star: pyrogenic aragonite from Tell es-Safi/Gath. Square: pyrogenic aragonite from Megiddo.

Based on the theoretical study of Poduska et al. [21] on calcite grinding curves and on the experimental study of Suzuki et al. [20] on geogenic, biogenic and synthetic aragonite grinding curves, we conclude that the most ordered aragonite crystals are the geogenic samples, whereas Lisan aragonite crystals are the least ordered. *Glycymeris* crystals are also well ordered at the atomic level and their curve overlaps with the geogenic curve, although part of it continues in the lower portion of the plot. This trend is caused by different starting particle size, since geogenic crystals are much larger than biogenic ones [20]. In addition, the *Glycymeris* curve starts below the geogenic one. This could be interpreted as a consequence of biogenic crystals being more ordered than the geogenic. However, a more parsimonious interpretation is that the curve is partially displaced below the geogenic reference due to the presence of amorphous calcium carbonate (ACC) in the mature shell [43–45]. Since we did not differentiate between layers within the shell and ground it as a whole, we suspect that sites with preserved ACC might contribute to the infrared absorptions of aragonite. It is known that ACC is characterized by split ν_3 peaks and extremely shallow ν_4 [46], which may affect the absorptions of mature aragonite crystals. Upon increased grinding, ACC turns into aragonite and this transformation shows up in the lower portion of the *Glycymeris* curve [20].

The kettle, pyrogenic and Lisan aragonite are less ordered, and this is probably due to their rapid growth rate. It is known that fast nucleation of carbonates in supersaturated solutions or after exposure to high temperatures favors the occurrence of defects in the crystal lattice [27,32,47]. Among the three, Lisan aragonite is characterized by the highest growth rate, as crystals precipitate almost immediately in supersaturated solutions [48]. This is consistent with previous finds reported

by Suzuki et al. [20], i.e., synthetic aragonite precipitated using magnesium as inhibitor is the least ordered material. Pyrogenic aragonite is slightly more ordered, probably because its growth rate is in the order of days in ash/quicklime, and weeks in the case of lime plaster [12]. Kettle aragonite precipitates rapidly in boiling water, and therefore it should be closer to the evaporitic form in terms of atomic order. However, the kinetics of this reaction are not well understood [11,49,50]. In addition, we cannot discount the possibility that aragonite crystals undergoing hundreds of boiling cycles in a kettle might grow along their *c*-axis and thus become more ordered. Indeed, some large crystals (>50 μm) were observed with SEM (Figure 2D).

3.2. Aragonite in Heat-Altered Sediments

The data presented in Figure 3 are consistent with results obtained by Suzuki et al. [20] for geogenic, biogenic, and synthetic aragonite. Pyrogenic aragonite appears to be entirely different from other known forms of the mineral and exhibits poor atomic order. This unique FTIR signature may thus be used to determine the presence of pyrogenic aragonite in sediments and carbonate-based materials. The validity of the pyrogenic aragonite grinding curve was tested using samples from archaeological combustion features where pyrogenic aragonite crystals were purified by density and identified by means of Raman micro-spectroscopy and SEM [35]. As shown in Figure 3, the plotted normalized heights of the samples from Megiddo and Tell es-Safi/Gath fall on the pyrogenic aragonite trendline. Thus, the grinding curve method for aragonite including the pyrogenic form offers a quick reference in the analysis of archaeological sediments using FTIR. The occurrence of pyrogenic aragonite has been determined with FTIR several times in archaeological combustion features and plasters [12,31,34–36]. However, the simultaneous presence of biogenic aragonite from shells, which is a common component of the archaeological record at many sites across the globe, requires a spectroscopic approach able to distinguish between the two. This becomes especially apparent in the case of combustion features where aragonite may be present as a byproduct of high-temperature burning of fuel and as shell fragments embedded in the sedimentary matrix [51,52]. The same applies to aragonitic shells embedded in lime mortars [53]. A swift calculation of the normalized heights may thus provide more accurate evidence and ultimately more solid interpretations.

3.3. Aragonite–Calcite Mixtures in Lime Binders

It has been shown that pyrogenic aragonite usually nucleates together with calcite, and that their relative amounts depend on the nature of the starting CaCO_3 substrate and environmental conditions during the carbonation process of magnesium-free CaO and $\text{Ca}(\text{OH})_2$ [12]. In the case of mixtures of pyrogenic aragonite and calcite in ash layers or lime plasters/mortars and concrete, part of the calcite might be secondary and derive from localized dissolution of aragonite (and/or calcite) and subsequent reprecipitation into calcite, following the thermodynamics of CaCO_3 at ambient conditions [3,11]. Instead, pyrogenic aragonite has proved to be a closed carbon system when preserved, based on radiocarbon dating of aragonite crystals from the Iron Age Megiddo destruction layer that yielded the same age range of charred seeds embedded within the same context [35]. Therefore, pyrogenic aragonite in archaeological materials appears to be pristine, whereas calcite might show different degrees of atomic order that may be important for interpretations regarding the integrity of the archaeological record and of present-day construction materials [2,3,54]. It would thus be useful to determine the degree of atomic order of calcite in materials where both polymorphs are present.

The OMNIC macro cannot process both polymorphs at the same time, as they share the ν_4 absorption and the ν_3 peaks overlap. To overcome this limit, we propose a new, simple method. The normalized ν_2 heights of calcite and aragonite are obtained by dividing the relevant intensities of the ν_2 absorptions by the intensity of the respective ν_3 absorption. In the case displayed in Figure 4, the ν_3 is split between aragonite and calcite because the two polymorphs are present in similar proportions. The ratios are thus 875/1420 for calcite and 856/1475 for aragonite. If one of the two polymorphs is dominant, the other would appear as a shoulder in the ν_3 . The same procedure cannot be applied to

the ν_4 absorption at 713 cm^{-1} , as it is exactly the same for both polymorphs. Therefore, we assume that the ν_4 intensity is similar for calcite and aragonite when they are ground to the same extent, regardless of atomic order. This may be the case based on the grinding curve plots of Regev et al. [19] and Suzuki et al. [20], where the ν_2 normalized heights of calcite and aragonite show considerable offset, whereas the ν_4 normalized heights cover a similar range of values. The normalized ν_4 range shown in Figure 3 is consistent with these previous studies. In addition, the absorptivity values of the ν_4 in calcite and aragonite are similar [55]. Thus, in an infrared spectrum with both polymorphs, the ν_4 intensity would be the sum of the intensities of the two. By knowing their amounts based on XRD quantification, it is possible to divide the ν_4 intensity accordingly and relate the portion of intensity to the relevant polymorph. We tested this assumption by preparing KBr pellets of aragonite and calcite spar in ratios of 50:50, 70:30, and 30:70, respectively (Table 1). Based on grinding curves by Regev et al. [19], the calcite spar sample that we used is poorly ordered compared to optical Iceland spar but offers a good clear-cut when plotting normalized heights. The sample shown in Figure 4 contains 50% calcite and 50% aragonite, meaning that 50% of the ν_4 intensity was used for the calculation of the calcite normalized ν_4 and 50% for the aragonite normalized ν_4 . The resulting normalized heights were plotted in the respective grinding curve plots, Regev et al. [19] for calcite and the present study for aragonite (Figure 5). Values fall on the poorly ordered calcite and ordered aragonite curves as expected. Similar results were obtained for other mixtures (Table 1 and Figure 5).

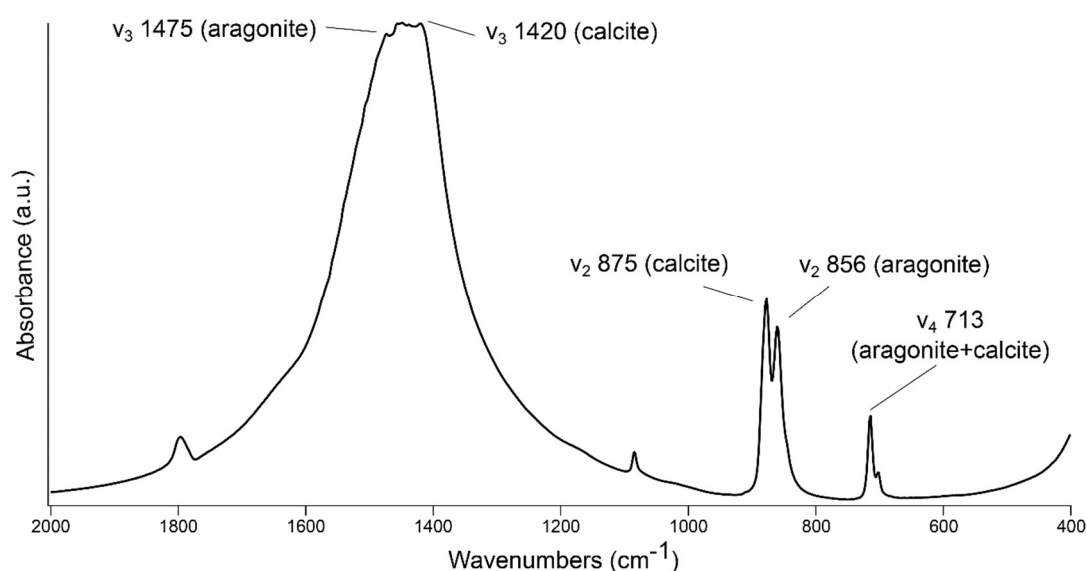


Figure 4. FTIR spectrum of a 50:50 mixture of calcite spar and aragonite spar, showing the location of the respective absorptions (a.u.: arbitrary units).

Table 1. Intensity values and normalized heights for calcite and aragonite in mixed polymorph samples (C: calcite; A: aragonite; N: normalized). The quantification of archaeological samples (C:A ratio) is based on XRD.

Sample and C:A Ratio (%)	Calcite					Aragonite				
	ν_3	ν_2	ν_4	N ν_2	N ν_4	ν_3	ν_2	ν_4	N ν_2	N ν_4
Mix 50:50	1.761	0.733	0.287	416	81	1.700	0.630	0.287	370	84
Mix 30:70	1.521	0.509	0.344	334	68	1.698	0.787	0.344	463	141
Mix 70:30	1.906	0.898	0.310	471	113	1.734	0.447	0.310	257	54
Megiddo coarse 40:60	0.086	0.028	0.017	325	79	0.149	0.060	0.017	402	68
Megiddo fine 30:70	0.353	0.147	0.075	416	70	0.703	0.324	0.075	460	71
Tell es-Safi/Gath 30:70	0.376	0.100	0.059	266	47	0.600	0.231	0.059	385	69
Motza 111 70:30	1.013	0.457	0.131	451	90	0.959	0.340	0.131	354	41
Motza 3889 80:20	1.264	0.532	0.147	420	93	1.198	0.354	0.147	295	24

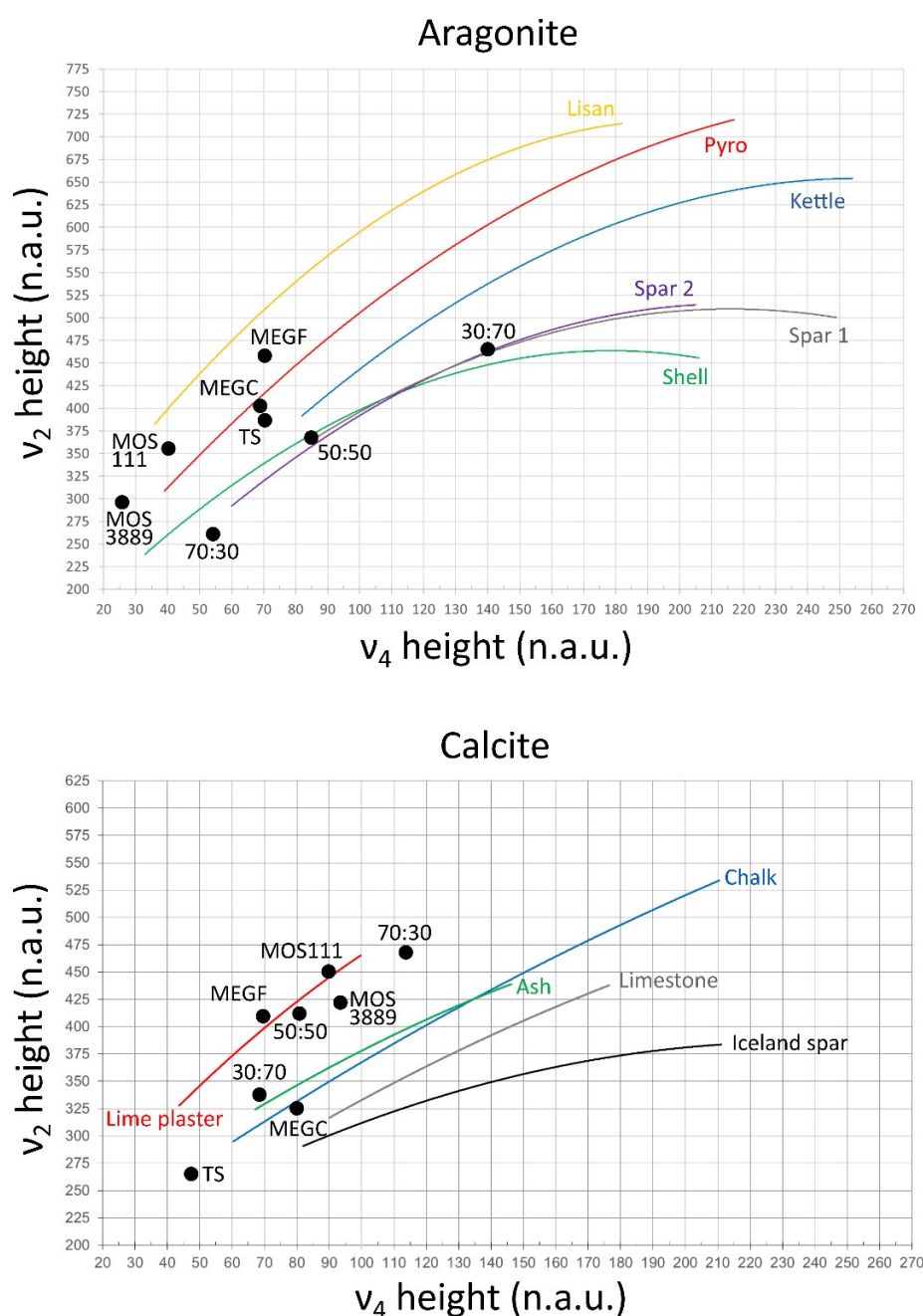


Figure 5. Aragonite and calcite grinding curve plots and location of experimental and archaeological samples (n.a.u.: normalized absorbance units). Calcite plot modified after Regev et al. (2010) [19]. MEGC: Megiddo coarse fraction; MEGF: Megiddo fine fraction; TS: Tell es-Safi/Gath; MOS: Motza. Ratios are calcite:aragonite.

3.4. Applications

The method presented above was tested with archaeological ash from Megiddo and Tell es-Safi/Gath and lime plasters from Motza, where quantification was performed using XRD. In all cases, the normalized v_2 and v_4 heights fall on the expected location in the curves of calcite and aragonite (Table 1 and Figure 5). Therefore, both ash layers are well preserved based on the poor atomic order shown by aragonite crystals. In addition, we obtained insights into the composition of these samples. More specifically, the Megiddo bulk sample, which should be richer in coarse particles of geogenic calcite based on a previous study [35], is indeed characterized by calcite that shows the

same degree of atomic order of chalk. Similarly, the ash from Tell es-Safi/Gath exhibits fairly ordered calcite located at the end of the chalk curve. This calcite derives from the local chalk bedrock [39].

The Neolithic plasters from Motza offered the opportunity to track the diagenetic history of the carbonate binder. MOS111 exhibits a good state of preservation of both aragonite and calcite, as suggested by the respective normalized heights located above the pyrogenic curves. Instead, plaster MOS3889, which comes from a different plaster floor within the site, exhibits more ordered calcite located below the lime plaster curve, which is indicative of recrystallization and thus diagenesis. Knowing that MOS111 contains a larger amount of aragonite, we hypothesize that in MOS3889 part of the aragonite might have recrystallized into calcite due to exposure to groundwater rich in carbonic acid. Therefore, by looking at different samples within the same site or architecture, it is possible to gain information on environmental settings affecting the preservation of the carbonate fraction at specific locales. We also observed a limitation in this method, i.e., for low amounts of either polymorph (ca. <15–20%) the ν_4 contribution becomes so small that it can be considered negligible. Therefore, in such cases it is possible to run the macro for single polymorphs to evaluate the preservation of the material.

The procedure presented herein finds two major applications. First, assessing the state of preservation of calcite and aragonite in lime binders may shed light on the properties of construction materials such as lime plaster, lime mortar, and concrete. Being more soluble than calcite, the nucleation of large amounts of aragonite may considerably affect the quality of binders and alter their mechanical and hydraulic behavior through dissolution and reprecipitation processes [18,56]. This includes also binders characterized by pozzolanic reactions, where aragonite is a common byproduct [57]. By determining the degree of atomic order of calcite in binders that contain also aragonite, it is possible to understand whether part of the calcite formed from the dissolution of aragonite and thus obtain an overall assessment of the integrity of the material. The same method could be applied to the characterization of nanolimes used in the restoration of works of art and cultural heritage during their carbonation process, as the addition of isopropyl alcohol to $\text{Ca}(\text{OH})_2$ promotes the nucleation of the metastable polymorphs of CaCO_3 , e.g., aragonite and vaterite [7,58]. These transient phases may persist through time or dissolve and lead to recrystallization if environmental conditions are unfavorable (e.g., exposure to rain water or humidity), thus affecting the integrity of the material.

Second, the proposed method can be used in radiocarbon dating of lime plaster/mortar from historical buildings. In the absence of short-lived charred organics embedded in these materials, the carbonate binder may offer a reliable source of ^{14}C for dating, provided that carbonates do not exchange carbon with the environment during burial or exposure to weathering agents through dissolution and reprecipitation processes triggered by carbonic acid [59]. When plasters/mortars contain both calcite and aragonite, it is possible to assess the state of preservation of calcite and select only poorly ordered samples for dating, as the latter are more likely to retain the original ^{14}C signature of the atmosphere at the time of carbonation of $\text{Ca}(\text{OH})_2$ [28]. This becomes especially important considering the possibility of separating carbonate fractions with different degrees of atomic order based on their specific gravity [35]. In addition, FTIR can rapidly identify microscopic fragments of aragonitic shells embedded in the lime binder, which are a source of contamination for radiocarbon dating, without using time-consuming methods such as thin section petrography [53].

4. Conclusions

Anthropogenic carbonates are pyrotechnological materials composed mainly of CaCO_3 , which may nucleate as calcite and/or aragonite. The degree of atomic order of different polymorphs may vary considerably depending on the state of preservation of the material, since differential dissolution may lead to the recrystallization of only part of the crystals. This is especially the case of archaeological materials such as ash and lime plaster/mortar that undergo burial conditions for thousands of years, and present-day concrete, mortar and plaster exposed to the elements. Being able to address these issues is particularly important for researchers who wish to develop reliable methods to decode the

diagenetic history of archaeological lime binders, in order to study novel conservation strategies. Here we presented a rapid method based on FTIR grinding curves of different aragonite standards that can determine the mechanism of formation of aragonite crystals of unknown origin, and in particular allows the identification of pyrogenic aragonite in archaeological combustion features where biogenic aragonite from shells may also occur. This method is based on changes in the normalized intensities of the ν_2 and ν_4 absorptions of aragonite upon repeated grinding of the KBr pellet, which depend on the degree of local structural order of the crystals and thus represent different formation processes. In addition, we proposed a method to assess separately the degree of atomic order of aragonite and calcite when both polymorphs occur in the same material. Since calcite and aragonite share exactly the same ν_4 absorption, but also exhibit similar infrared absorptivity, it is possible to quantify the contribution of each polymorph to the ν_4 vibration based on their quantification using XRD. Then, each ν_4 height can be used to locate calcite and aragonite on their relative grinding curve plots. This procedure finds applications in the characterization of the mechanical properties of construction and building materials based on lime binders, and in the identification of poorly ordered calcite for radiocarbon dating of archaeological lime plaster/mortar.

Author Contributions: Conceptualization, M.B.T.; Data curation, M.B.T., L.R., S.D., Y.L. and E.B.; Formal analysis, M.B.T., L.R., S.D., Y.L. and E.B.; Funding acquisition, M.B.T. and E.B.; Investigation, M.B.T., L.R., S.D. and Y.L.; Methodology, M.B.T.; Project administration, M.B.T.; Resources, M.B.T.; Software, M.B.T.; Supervision, M.B.T.; Validation, M.B.T., L.R., S.D., Y.L. and E.B.; Visualization, M.B.T.; Writing—original draft, M.B.T.; Writing—review and editing, M.B.T., L.R., S.D., Y.L. and E.B.

Funding: This research was funded by IdEx Bordeaux, grant number ANR-10-IDEX-03-02 to Michael Toffolo, and by the Exilarch's Foundation for the Dangoor Research Accelerator Mass Spectrometer (D-REAMS). Elisabetta Boaretto is the incumbent of the Dangoor Professorial Chair of Archaeological Sciences. The APC was funded by IdEx Bordeaux, grant number ANR-10-IDEX-03-02 to Michael Toffolo.

Acknowledgments: The authors wish to thank Steve Weiner, who kindly provided samples of kettle and Lisan aragonite; Israel Finkelstein for samples of aragonitic ash from Megiddo; Aren Maier for samples of aragonitic ash from Tell es-Safi/Gath; Hamoudi Khalaily for samples of lime plaster from Motza. The authors are grateful to Anne Delagnes, Francesco d'Errico and Alain Queffelec for granting access to laboratory equipment at PACEA, Université de Bordeaux.

Conflicts of Interest: The authors declare no conflict of interest. The funders had no role in the design of the study; in the collection, analyses, or interpretation of data; in the writing of the manuscript, or in the decision to publish the results.

References

1. Boynton, R.S. *Chemistry and Technology of Lime and Limestone*; John Wiley & Sons, Inc.: New York, NY, USA, 1980.
2. Artioli, G. *Scientific Methods and Cultural Heritage: An Introduction to the Application of Materials Science to Archaeometry and Conservation Science*; Oxford University Press: Oxford, UK, 2010.
3. Weiner, S. *Microarchaeology: Beyond the Visible Archaeological Record*; Cambridge University Press: New York, NY, USA, 2010.
4. Pöllmann, H. *Cementitious Materials: Composition, Properties, Application*; De Gruyter: Berlin, Germany, 2017.
5. Kingery, W.D.; Vandiver, P.B.; Prickett, M. The beginnings of pyrotechnology, part II: Production and use of lime and gypsum plaster in the Pre-Pottery Neolithic Near East. *J. Field Archaeol.* **1988**, *15*, 219–244. [[CrossRef](#)]
6. Berna, F.; Goldberg, P.; Kolska Horwitz, L.; Brink, J.; Holt, S.; Bamford, M.; Chazan, M. Microstratigraphic evidence of in situ fire in the Acheulean strata of Wonderwerk Cave, Northern Cape province, South Africa. *Proc. Natl. Acad. Sci. USA* **2012**, *109*, E1215–E1220. [[CrossRef](#)] [[PubMed](#)]
7. Rodriguez-Navarro, C.; Ruiz-Agudo, E. Nanolimes: From synthesis to application. *Pure Appl. Chem.* **2018**, *90*, 523–550. [[CrossRef](#)]
8. Papayianni, I.; Pachta, V.; Stefanidou, M. Analysis of ancient mortars and design of compatible repair mortars: The case study of Odeion of the archaeological site of Dion. *Constr. Build. Mater.* **2013**, *40*, 84–92. [[CrossRef](#)]

9. Izzo, F.; Arizzi, A.; Cappelletti, P.; Cultrone, G.; De Bonis, A.; Germinario, C.; Graziano, S.F.; Grifa, C.; Guarino, V.; Mercurio, M.; et al. The art of building in the Roman period (89 BC–79 AD): Mortars, plasters and mosaic floors from ancient *Stabiae* (Naples, Italy). *Constr. Build. Mater.* **2016**, *117*, 129–143. [[CrossRef](#)]
10. Secco, M.; Dilaria, S.; Addis, A.; Bonetto, J.; Artioli, G.; Salvadori, M. The evolution of the Vitruvian recipes over 500 years of floor-making techniques: The case studies of the *Domus delle Bestie Ferite* and the *Domus di Tito Macro* (Aquileia, Italy). *Archaeometry* **2018**, *60*, 185–206. [[CrossRef](#)]
11. Lippmann, F. *Sedimentary Carbonate Minerals*; Springer: Heidelberg, Germany, 1973.
12. Toffolo, M.B.; Boaretto, E. Nucleation of aragonite upon carbonation of calcium oxide and calcium hydroxide at ambient temperatures and pressures: A new indicator of fire-related human activities. *J. Archaeol. Sci.* **2014**, *49*, 237–248. [[CrossRef](#)]
13. Lowenstam, H.A.; Weiner, S. *On Biomineralization*; Oxford University Press: New York, NY, USA, 1989.
14. Pokroy, B.; Fitch, A.; Zolotoyabko, E. The microstructure of biogenic calcite: A view by high-resolution synchrotron powder diffraction. *Adv. Mater.* **2006**, *18*, 2363–2368. [[CrossRef](#)]
15. Pokroy, B.; Quintana, J.P.; Caspi, E.N.; Berner, A.; Zolotoyabko, E. Anisotropic lattice distortions in biogenic aragonite. *Nat. Mater.* **2004**, *3*, 900–902. [[CrossRef](#)]
16. Politi, Y.; Metzler, R.A.; Abrecht, M.; Gilbert, B.; Wilt, F.H.; Sagi, I.; Addadi, L.; Weiner, S.; Gilbert, P.U.P.A. Transformation mechanism of amorphous calcium carbonate into calcite in the sea urchin larval spicule. *Proc. Natl. Acad. Sci. USA* **2008**, *105*, 17362–17366. [[CrossRef](#)]
17. Zolotoyabko, E.; Caspi, E.N.; Fieramosca, J.S.; Von Dreele, R.B.; Marin, F.; Mor, G.; Addadi, L.; Weiner, S.; Politi, Y. Differences between bond lengths in biogenic and geological calcite. *Cryst. Growth Des.* **2010**, *10*, 1207–1214. [[CrossRef](#)]
18. Gómez-Villalba, L.S.; López-Arce, P.; Álvarez de Buergo, M.; Fort, R. Atomic defects and their relationship to aragonite-calcite transformation in portlandite nanocrystal carbonation. *Cryst. Growth Des.* **2012**, *12*, 4844–4852. [[CrossRef](#)]
19. Regev, L.; Poduska, K.M.; Addadi, L.; Weiner, S.; Boaretto, E. Distinguishing between calcites formed by different mechanisms using infrared spectrometry: Archaeological applications. *J. Archaeol. Sci.* **2010**, *37*, 3022–3029. [[CrossRef](#)]
20. Suzuki, M.; Dauphin, Y.; Addadi, L.; Weiner, S. Atomic order of aragonite crystals formed by mollusks. *CrystEngComm* **2011**, *13*, 6780–6786. [[CrossRef](#)]
21. Poduska, K.M.; Regev, L.; Boaretto, E.; Addadi, L.; Weiner, S.; Kronik, L.; Curtarolo, S. Decoupling local disorder and optical effects in infrared spectra: Differentiating between calcites with different origins. *Adv. Mater.* **2011**, *23*, 550–554. [[CrossRef](#)]
22. Khalifa, G.M.; Weiner, S.; Addadi, L. Mineral and matrix components of the operculum and shell of the barnacle *Balanus amphitrite*: Calcite crystal growth in a hydrogel. *Cryst. Growth Des.* **2011**, *11*, 5122–5130. [[CrossRef](#)]
23. Kim, Y.-Y.; Ganesan, K.; Yang, P.; Kulak, A.N.; Borukhin, S.; Pechook, S.; Ribeiro, L.; Kröger, R.; Eichhorn, S.J.; Armes, S.P.; et al. An artificial biomineral formed by incorporation of copolymer micelles in calcite crystals. *Nat. Mater.* **2011**, *10*, 890–896. [[CrossRef](#)] [[PubMed](#)]
24. Di Benedetto, F.; Bucciatti, A.; Montegrossi, G.; Innocenti, M.; Massa, C.A.; Pardi, L.A.; Romanelli, M. EPR discrimination of microcrystalline calcite geomaterials. *Am. Mineral.* **2012**, *97*, 1619–1626. [[CrossRef](#)]
25. Bonacini, I.; Prati, S.; Mazzeo, R.; Falini, G. Crystallization of CaCO₃ in the presence of ethanolamine reveals transient meso-like crystals. *Cryst. Growth Des.* **2014**, *14*, 5922–5928. [[CrossRef](#)]
26. Falini, G.; Fermani, S.; Reggi, M.; Džakula, B.N.; Kralj, D. Evidence of structural variability among synthetic and biogenic vaterite. *Chem. Commun.* **2014**, *50*, 15370–15373. [[CrossRef](#)] [[PubMed](#)]
27. Xu, B.; Toffolo, M.B.; Boaretto, E.; Poduska, K.M. Assessing local and long-range structural disorder in aggregate-free lime binders. *Ind. Eng. Chem. Res.* **2016**, *55*, 8334–8340. [[CrossRef](#)]
28. Poduska, K.M.; Regev, L.; Berna, F.; Mintz, E.; Milevski, I.; Khalaily, H.; Weiner, S.; Boaretto, E. Plaster characterization at the PPNB site of Yiftahel (Israel) including the use of ¹⁴C: Implications for plaster production, preservation, and dating. *Radiocarbon* **2012**, *54*, 887–896. [[CrossRef](#)]
29. Regev, L.; Eckmeier, E.; Mintz, E.; Weiner, S.; Boaretto, E. Radiocarbon concentrations of wood ash calcite: Potential for dating. *Radiocarbon* **2011**, *53*, 117–127. [[CrossRef](#)]
30. Regev, L.; Zukerman, A.; Hitchcock, L.; Maeir, A.M.; Weiner, S.; Boaretto, E. Iron Age hydraulic plaster from Tell es-Safi/Gath, Israel. *J. Archaeol. Sci.* **2010**, *37*, 3000–3009. [[CrossRef](#)]

31. Regev, L.; Cabanes, D.; Homsher, R.; Kleiman, A.; Weiner, S.; Finkelstein, I.; Shahack-Gross, R. Geoarchaeological investigation in a domestic Iron Age quarter, Tel Megiddo, Israel. *Bull. Am. Sch. Orient. Res.* **2015**, *374*, 135–157. [[CrossRef](#)]
32. Xu, B.; Toffolo, M.B.; Regev, L.; Boaretto, E.; Poduska, K.M. Structural differences in archaeologically relevant calcite. *Anal. Methods* **2015**, *7*, 9304–9309. [[CrossRef](#)]
33. Toffolo, M.B.; Ullman, M.; Caracuta, V.; Weiner, S.; Boaretto, E. A 10,400-year-old sunken lime kiln from the Early Pre-Pottery Neolithic B at the Neshar-Ramla quarry (el-Khirbe), Israel. *J. Archaeol. Sci. Rep.* **2017**, *14*, 353–364. [[CrossRef](#)]
34. Asscher, Y.; Lehmann, G.; Rosen, S.A.; Weiner, S.; Boaretto, E. Absolute dating of the Late Bronze to Iron Age transition and the appearance of Philistine culture in Qubur el-Walaydah, southern Levant. *Radiocarbon* **2015**, *57*, 77–97. [[CrossRef](#)]
35. Toffolo, M.B.; Regev, L.; Mintz, E.; Poduska, K.M.; Shahack-Gross, R.; Berthold, C.; Miller, C.E.; Boaretto, E. Accurate radiocarbon dating of archaeological ash using pyrogenic aragonite. *Radiocarbon* **2017**, *59*, 231–249. [[CrossRef](#)]
36. Eliyahu-Behar, A.; Yahalom-Mack, N.; Ben-Shlomo, D. Excavation and analysis of an early Iron Age lime kiln. *Isr. Explor. J.* **2017**, *67*, 14–31.
37. Sivan, D.; Potasman, M.; Almogi-Labin, A.; Bar-Yosef Mayer, D.E.; Spanier, E.; Boaretto, E. The *Glycymeris* query along the coast and shallow shelf of Israel, southeast Mediterranean. *Palaeogeogr. Palaeoclimatol. Palaeoecol.* **2006**, *233*, 134–148. [[CrossRef](#)]
38. Bartov, Y.; Stein, M.; Enzel, Y.; Agnon, A.; Reches, Z. Lake levels and sequence stratigraphy of Lake Lisan, the late Pleistocene precursor of the Dead Sea. *Quat. Res.* **2002**, *57*, 9–21. [[CrossRef](#)]
39. Toffolo, M.; Maeir, A.M.; Chadwick, J.R.; Boaretto, E. Characterization of contexts for radiocarbon dating: Results from the early Iron Age at Tell es-Safi/Gath, Israel. *Radiocarbon* **2012**, *54*, 371–390. [[CrossRef](#)]
40. Maeir, A.M. Chapter 1: The Tell es-Safi/Gath archaeological project 1996–2010: Introduction, overview and synopsis of results. In *Tell Es-Safi/Gath I: Report on the 1996–2005 Seasons*; Maeir, A.M., Ed.; Harrassowitz: Wiesbaden, Germany, 2012.
41. Khalaily, H.; Bar-Yosef, O.; Barzilai, O.; Boaretto, E.; Bocquentin, F.; Eirikh-Rose, A.; Greenhut, Z.; Goring-Morris, A.N.; Le Dosseur, G.; Marder, O.; et al. Excavations at Motza in the Judean Hills and The Early Pre-Pottery Neolithic B in the Southern Levant. *Paléorient* **2007**, *33*, 5–37. [[CrossRef](#)]
42. Farmer, V.C. *The Infrared Spectra of Minerals*; Mineralogical Society: London, UK, 1974.
43. Weiss, I.M.; Tuross, N.; Addadi, L.; Weiner, S. Mollusc larval shell formation: Amorphous calcium carbonate is a precursor phase for aragonite. *J. Exp. Zool.* **2002**, *293*, 478–491. [[CrossRef](#)] [[PubMed](#)]
44. Addadi, L.; Raz, S.; Weiner, S. Taking advantage of disorder: Amorphous calcium carbonate and its roles in biomineralization. *Adv. Mater.* **2003**, *15*, 959–970. [[CrossRef](#)]
45. Koishi, A.; Fernandez-Martinez, A.; Ruta, B.; Jimenez-Ruiz, M.; Poloni, R.; di Tommaso, D.; Zontone, F.; Waychunas, G.A.; Montes-Hernandez, G. Role of impurities in the kinetic persistence of amorphous calcium carbonate: A nanoscopic dynamics view. *J. Phys. Chem. C* **2018**, *122*, 16983–16991. [[CrossRef](#)]
46. Beniash, E.; Aizenberg, J.; Addadi, L.; Weiner, S. Amorphous calcium carbonate transforms into calcite during sea urchin larval spicule growth. *Proc. R. Soc. Lond. B* **1997**, *264*, 461–465. [[CrossRef](#)]
47. Teng, H.H.; Dove, P.M.; De Yoreo, J.J. Kinetics of calcite growth: Surface processes and relationships to macroscopic rate laws. *Geochim. Cosmochim. Acta* **2000**, *64*, 2255–2266. [[CrossRef](#)]
48. Goodarz-Nia, I.; Motamedi, M. Kinetics of calcium carbonate crystallization from aqueous solutions. *J. Cryst. Growth* **1980**, *48*, 125–131. [[CrossRef](#)]
49. Goto, M. Some mineralo-chemical problems concerning calcite and aragonite, with special reference to the genesis of aragonite. *J. Fac. Sci. Hokkaido Univ. Ser.* **1961**, *10*, 571–640.
50. Jones, B. Review of calcium carbonate polymorph precipitation in spring systems. *Sediment. Geol.* **2017**, *353*, 64–75. [[CrossRef](#)]
51. Albert, R.M.; Shahack-Gross, R.; Cabanes, D.; Gilboa, A.; Lev-Yadun, S.; Portillo, M.; Sharon, I.; Boaretto, E.; Weiner, S. Phytolith-rich layers from the Late Bronze and Iron Ages at Tel Dor (Israel): Mode of formation and archaeological significance. *J. Archaeol. Sci.* **2008**, *35*, 57–75. [[CrossRef](#)]

52. Esteban, I.; Marean, C.W.; Fisher, E.C.; Karkanas, P.; Cabanes, D.; Albert, R.M. Phytoliths as an indicator of early modern humans plant gathering strategies, fire fuel and site occupation intensity during the Middle Stone Age at Pinnacle Point 5–6 (south coast, South Africa). *PLoS ONE* **2018**, *13*, e0198558. [[CrossRef](#)] [[PubMed](#)]
53. Riquelme, F.; Alvarado-Ortega, J.; Cuevas-García, M.; Ruvalcaba-Sil, J.L.; Linares-López, C. Calcareous fossil inclusions and rock-source of Maya lime plaster from the Temple of the Inscriptions, Palenque, Mexico. *J. Archaeol. Sci.* **2012**, *39*, 624–639. [[CrossRef](#)]
54. Weiner, S.; Goldberg, P.; Bar-Yosef, O. Three-dimensional distribution of minerals in the sediments of Hayonim Cave, Israel: Diagenetic processes and archaeological implications. *J. Archaeol. Sci.* **2002**, *29*, 1289–1308. [[CrossRef](#)]
55. Vagenas, N.V.; Gatsouli, A.; Kontoyannis, C.G. Quantitative analysis of synthetic calcium carbonate polymorphs using FT-IR spectroscopy. *Talanta* **2003**, *59*, 831–836. [[CrossRef](#)]
56. Fernández-Carrasco, L.; Torréns-Martín, D.; Martínez-Ramírez, S. Carbonation of ternary building cementing materials. *Cem. Concr. Compos.* **2012**, *34*, 1180–1186. [[CrossRef](#)]
57. Jackson, M.D. Sea-water concretes and their material characteristics. In *Building for Eternity*; Brandon, C.J., Hohlfelder, R.L., Jackson, M.D., Oleson, J.P., Eds.; Oxbow Books: Oxford, UK, 2014; pp. 141–187.
58. Sand, K.K.; Rodriguez-Blanco, J.D.; Makovicky, E.; Benning, L.G.; Stipp, S.L.S. Crystallization of CaCO₃ in water-alcohol mixtures: Spherulitic growth, polymorph stabilization, and morphology change. *Cryst. Growth Des.* **2011**, *12*, 842–853. [[CrossRef](#)]
59. Boaretto, E.; Poduska, K.M. Materials science challenges in radiocarbon dating: The case of archaeological plasters. *J. Miner. Met. Mater. Soc. TMS* **2013**, *65*, 481–488. [[CrossRef](#)]



© 2019 by the authors. Licensee MDPI, Basel, Switzerland. This article is an open access article distributed under the terms and conditions of the Creative Commons Attribution (CC BY) license (<http://creativecommons.org/licenses/by/4.0/>).